International Journal of Electronics Engineering (ISSN: 0973-7383
Volume 11 • Issue 2 pp. 433-440 June 2019-Dec 2019 www.csjournals.com

Hydrothermal synthesis of Sb-incorporated SnO_2 nanoparticles for promising gas sensor applications

Davender Singh[1], Virender Singh Kundu[2], Mahesh K. Yadav[4] Jitendra Gangwar[1] A. S. Maan[3]
[1]*Department of Physics, RPS Degree College, Balana, Mahendergarh- 123029, India*
[2]*Department of Electronic Science, Kurukshetra University, Kurukshetra -136 119, India*
[3]*Department of Physics, Maharshi Dayanand University, Rohtak- 124 001, India*
[4]*Department of Electronics, RPS College of Engineering and Technology, Balana, Mahendergarh- 123029, India*

Abstract: Sb-doped SnO_2 nanoparticles were synthesized successfully by hydrothermal technique with different doping concentration of antimony. SnO_2 calcined nanoparticles at 400^0C were characterized by means of X-ray diffraction (XRD). XRD analyses revealed that nanoparticles of different doping concentration are polycrystalline in nature and existed as tetragonal rutile structure. Particle size of nanoparticles was calculated by using Scherrer formula and was found in the range of 7-21 nm. Morphology and nature of nanoparticles were analyzed by using scanning electron microscope (SEM), study of images confirmed the existence of very small, crystalline, uniformly distributed and spherical in shape nanoparticles. EDX analysis confirmed the proper incorporation of antimony atoms and presence of oxygen and tin. FTIR study confirmed the formation of Sn–O phase and hydrous nature of Sb-doped SnO_2 nanoparticles. The gas sensing properties were investigated for various concentrations of hydrogen sulphide (H_2S) and ammonia (NH_3) at different operating temperatures. x=0.20 Sb-doped shows the maximum response 64 % to hydrogen sulphide (H_2S), and 71% to ammonia (NH_3) respectively at different operating temperature within the measurement limit for a concentration of 100 ppm of each gases.
Key words: Sb-SnO_2; Nanoparticles; Hydrothermal; XRD; SEM; Gas sensing response.

1. INTRODUCTION

Nanomaterials have drawn great interest due to their exciting properties, which are different from those of their corresponding bulk part. The ongoing trends toward tininess has linked with small cost techniques and have need of preparation methods with refined control on the size and shape of particles. Controlled synthesis of nanostructures is an essential step for production of nanodevices. Performance of semiconductor nanodevices may depend on their morphology. Semiconductor oxide nanostructures proved significant properties, thermal and chemical stability, diverse functionalities, durability, and towards high degree of crystallinity. Therefore, it will be of elementary and technological attention to develop simplistic and valuable methods to get organized metal oxide nanostructures with fine shape and size control. Tin oxide (SnO_2) is possibly one of the most exciting materials that have to be investigated today. It has various distinctive properties for diverse cutting-edge applications varying from gas sensing to catalyst and optical electronic devices [1-6]. Thus, it is very significant to develop different ways for controlling their various morphological properties e.g. dimensions, structure, surface, and interface properties. It has been investigated by various researchers that by doping of various elements and also by different methodology to grow nanoparticles the basic properties of tin oxide can be modified [7-13]. Huang et al. fabricated film type nanowire sensors based on Sb-doped SnO_2 single crystalline nanowires and found that they exhibited faster response and recovery compared to sensors based on un-doped SnO_2 nanowires [14]. Jeon et al. [15] showed that conductivity of antimony tin oxide (ATO) film increases up to 80^0C but do not show any rise further to temperature above 1000^0C, the best conductivity was found for the ratio of antimony and tin was 1.5: 8.5. Binding energy increased amazingly at 1000^0C calcinations and the normal grain size was spread within a 5 nm (at 400^0C) to 50 nm (at 1000^0C) range. Bai et al. [16] showed Sb-doped stage of nanostructures and the degree of crystallinity are improved as compared with that at continually high temperature also ATO nanoparticles show a superior dispersibility, as most of them have a ranging of size from 10nm to 15nm. Kong et al. [17] with antimony-doped tin oxide (SnO_2: Sb), thin films explained that layers of films, annealing process and doping of Sb all influence optical constants, refraction index, grain size, and extinction coefficient. Babar et al. [18] showed that the effect of molar concentration of Sb: SnO_2 nanostructures decreased the optical band gap from 3.60 to 3.50 eV and it becomes sensitive to acetone, ethanol and LPG. In this present article, the author synthesized Sb-SnO_2 nanoparticles by Hydrothermal method as this method has some benefits over the others such as low temperature synthesis, high purity and high chemical homogeneity.

2. EXPERIMENTAL

2.1 Synthesis of pure and Sb-doped SnO_2 (Sb: SnO_2)

Pure and Sb-doped SnO_2 nanoparticles have been synthesized by hydrothermal technique. Tin chloride (Hydrous $SnCl_4.5H_2O$ 99% Merck, Germany) and antimony chloride ($SbCl_3$, 99% Merck, Germany) of AR grades have been used as starting material for the synthesis of Sb -doped tin oxide nanoparticles. xSb(1-x) SnO_2 (with various mol % of x =0, 0.05. 0.10, 0.15 and 0.20) nanopowders were successfully prepared by dissolving required amount of $SnCl_4.5H_2O$ and $SbCl_3$ in 50 ml DI(de-ionized) water separately, that was followed by the addition of solution of $SbCl_3$ drop wise to the solution of $SnCl_4.5H_2O$ under constant stirring at 60-70°C for 90 minute. The sufficient amount of aqueous ammonia (NH_4OH) has added to the above solution as reducing agent till the formation of perfect gel. The dropping rate must be well controlled for chemical homogeneity. The gel was transferred to teflon lined stainless steel autoclave and the heating treatment of synthesized nanoparticles were conducted at 100^0C for 18 hours. The gel was filtered and washed (3-4 times) to remove impurities and dried at 80^0C for 6-7 hours in order to remove water molecules Finally, Sb-doped tin oxide nanopowders were obtained after calcinations of dried gel at 400^0C for 5 hours.

2.1 Characterization

2.2.1. Structural and morphological characterization

The detailed characterization of the as obtained annealed samples was carried out using XRD, SEM with EDX, FTIR and gas sensing instruments.

The XRD patterns were taken by using Rigaku X-ray diffractometer with Cu Kα X-ray source having fixed wavelength, λ= 1.5406 Å radiation at 2θ values between 20^0 and 70^0.

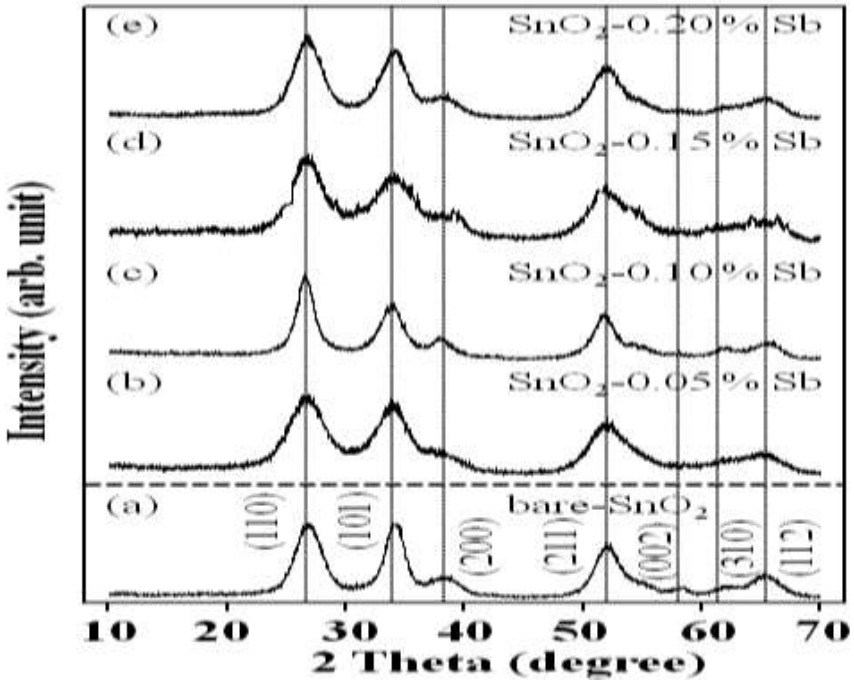

Fig.1 Spectra of bare SnO_2 and Sb incorporated SnO_2 nanoparticles

The average crystallite size is estimated using the FWHM of peaks based on Scherrer's equation [19, 20].

$$D = 0.94 \lambda / \beta \cos \theta$$

Where D is the average crystallite domain size perpendicular to the reflecting planes, λ is wavelength (1.5406 Å) of X-rays used, β is the broadening of diffraction line measured at half of its maximum intensity (in radian), full width at half maximum, and θ is the angle of diffraction.

The surface morphology was observed by Scanning Electron Microscope (SEM) and the compositions of Sb-doped SnO_2 were examined by EDX as shown in fig.2.

International Journal of Electronics Engineering (ISSN: 0973-7383
Volume 11 • Issue 2 pp. 433-440 June 2019-Dec 2019 www.csjournals.com

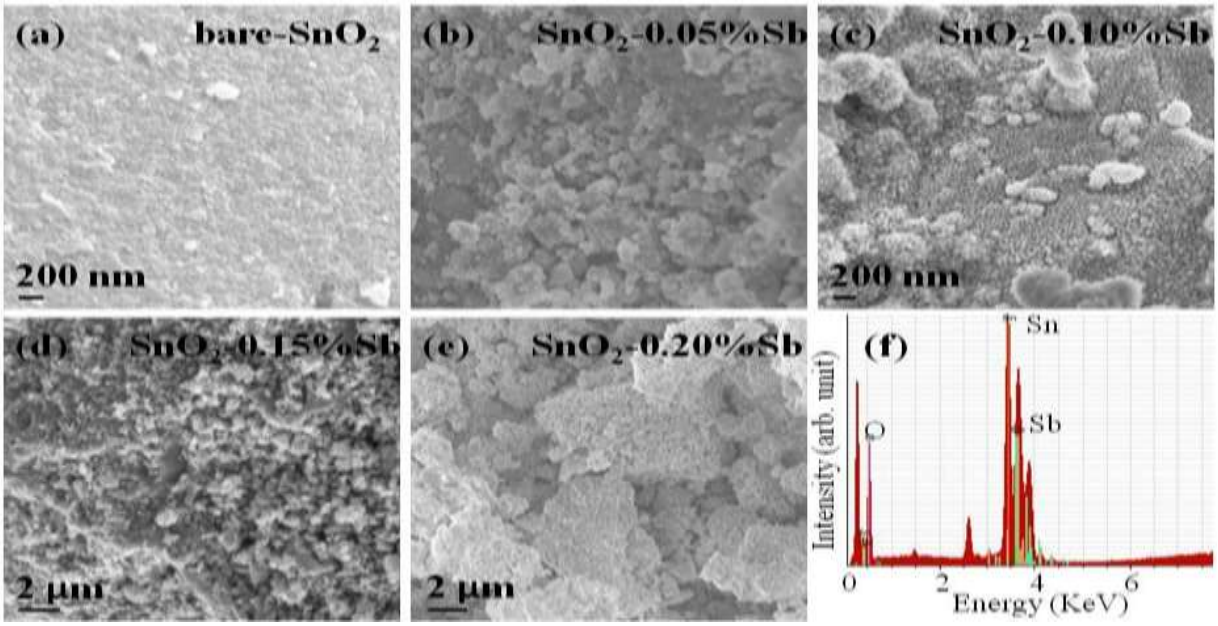

Fig.2 Microstructure of: (a) bare-SnO_2, (b) 0.05%Sb-SnO_2, (c) 0.10%Sb-SnO_2, (d) 0.15% Sb-SnO_2, (e) 0.20% Sb-SnO_2, and (f) EDX spectrum of Sb-incorporated SnO_2 Nanoparticles

The FTIR spectra within range 500-4000 $cm^{-1}$of bare and Sb-doped SnO_2 are shown in Fig.3. FTIR analysis was done with the help of Thermo Scientific model no.Nicolet^{TM} iS^{TM} 50 FT-IR spectrometer over the range 500-2000 cm^{-1}.

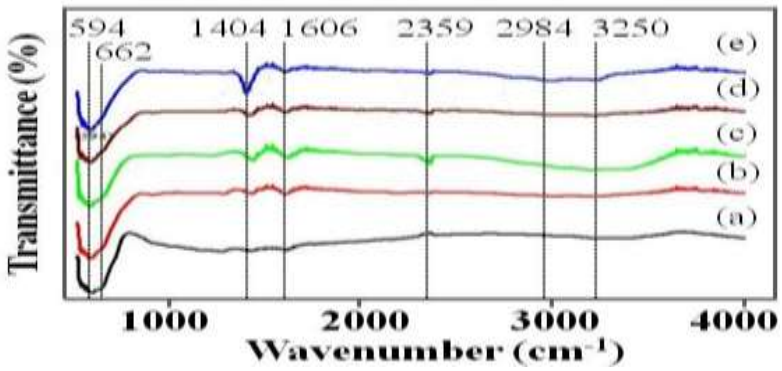

Fig.3 FTIR spectra of bare SnO_2 and Sb incorporated SnO_2 nanoparticles

2.2.2. Sensing characterization

To study the gas sensing behaviour of samples, the fine powders of both, pure and Sb-doped tin oxide samples were pressed into pellets of 10 mm diameter and 2.5 mm thickness at a pressure of 25 Mpa separately using a hydraulic press. These pellets were calcinated at around 500^0C for 2h in air and then both side faces were polished and coated with conducting silver paste used for making ohmic contacts on the two flat surfaces of pellets. For electrical measurements, pellet was mounted in a specially designed chamber (home-made two-probe assembly) which was inserted coaxially inside a resistance-heated furnace. The fixed amount of hydrogen sulphide (H_2S) and ammonia (NH_3) gases were injected into chamber of gas sensing system where sensor was placed. The dc resistance of sample was measured using a Keithley-617 electrometer. The sensor characteristics were recorded by measuring resistance in presence of gas and in air at different temperatures in the range 50-300^0C. The concentration of gas and temperature of chamber are measured by mass flow meters and a thermocouple (K-type Chromal-Alumna) respectively, attached to the sensor.

The gas sensitivity of pure and Sb-doped SnO_2 pallets was measured for different concentration of gases at different temperature. The 50 and 100 ppm of hydrogen sulphide (H_2S) and ammonia (NH_3) gases were used as target gases. Initially the resistance of pallets was determined in presence of air. On exposing pellet samples to these target gases,

pellet resistance was found to decrease for all these two gases. Sensor response (S) has been defined as the ratio of change in pellet resistance to pellet resistance in air (at constant temperature) and is given by the equation [21].

$$S = \frac{R_a - R_g}{R_a} \times 100\,\%$$

Where R_a is resistance of pellet in air and R_g is the resistance of pallet in presence of gas under study.

3. RESULTS AND DISCUSION

3.1 X-ray diffraction analysis

The XRD patterns of as synthesized pure and Sb-doped SnO_2 nanoparticles were recorded and shown in fig.1. The observed pattern has a number of sharp peaks at (110), (101), (200), (211), (002), (310) and (112) at different angles (2θ). The sharpness of the diffraction peaks reflect the degree of crystallinity. The position of peaks of pure as well as Sb-doped SnO_2 nanoparticles agree well with the diffraction of rutile SnO_2 crystals, which are also in consistent with the previous results [22, 23]. All the diff raction peaks indexed to rutile tetragonal structure of SnO_2 with lattice parameters a = b = 4.742 Å and c = 3.190Å which is consistent with the standard data (JCPDS file No. 77-0449) for SnO_2. Any secondary phase e.g. SnO or Sb_2O_3 was not observed that suggest the complete formation of a solid solution with all the Sb ions being substituted for Sn ions in the lattice. With increase in doping of Sb it has been observed that the sharpness of the diffraction peaks decreased and width of the diffraction peaks of Sb-doped SnO_2 increased which denotes a decrease in average particle size. We can see that the sizes of pure SnO_2 crystals are larger than that of Sb doped SnO_2 crystals.

The average crystallite size along (110) & (101) peaks decreases from 21 to 7 nm with increase in doping of Sb from x = 0.05 to 0.20% as also these results confirmed with observed earlier by Krishna kumar et al. [24] and Geraldo et al. [25]. The comparative analysis of average crystalline size along (110) & (101) peaks is given in table no.1.

Table 1 X-ray powder diffraction analysis of bare-SnO_2 and Sb-incorporated SnO_2 nanoparticles corresponding to the (110) and (101) diffraction peaks.

Samples x.Sb (1-x).SnO_2	**2 theta (degree)**	**d-spacing (Å)**	**(h k l) values**	**Average Crystal size (D nm)**
x = 0.00	26.73	3.32	(1 1 0)	21
	34.18	2.52	(1 0 1)	18
x = 0.05	26.75	3.33	(1 1 0)	16
	33.93	2.63	(1 0 1)	14
x = 0.10	26.60	3.34	(1 1 0)	15
	34.09	2.63	(1 0 1)	14
x = 0.15	26.54	3.36	(1 1 0)	12
	33.82	2.65	(1 0 1)	10
x = 0.20	25.12	3.53	(1 1 0)	11
	32.75	2.74	(1 0 1)	07

3.2 SEM and EDX analysis:

Scanning electron microscopy (SEM) provided further insight into the morphology and size details of the tin oxide nanoparticles. The SEM images of as-synthesized pure and Sb-doped SnO_2 nanoparticle samples are shown in given fig.2. It can be seen that pure SnO_2 nanomaterials possess uniform grains and is almost homogeneously distributed, which indicates the high packing density of these particles. It can be understood easily that the as prepared SnO_2 particles are fine and some agglomeration of finer particulates to form bigger clusters. Particle size and distribution of nanoparticles mainly depend upon the relative rates of nucleation and growth processes, as well as the extent of agglomeration [26].

However, there is some non-uniformity in the shape and the existence of porosity. On increasing the concentration of Sb doping, the surface morphology of the nanomaterials changes continuously and the grains also deteriorate. Also any phase aggregation was not observed other than the decrease in particle /grain size due to Sb doping. The observation obtained from SEM analysis also supports the XRD results and confirms the transition, crystalline state to amorphous state for higher Sb concentrations. EDX analysis also confirms that as prepared nanomaterials are

composed of three kinds of elements O, Sn and Sb. This means that Sb atoms are properly incorporated in Sb-doped SnO_2 properly.

3.3 FTIR Analysis:

The un-doped SnO_2 has its main peaks at 594cm^{-1} and at 662 cm^{-1}. The broad bands between 500 and 700 cm^{-1} are attributed to the framework vibrations of the Sn–O bond in SnO_2 [27, 28]. The peak appearing at 594 cm^{-1} is due to the terminal oxygen vibration of Sn–OH. The peak appeared at 662 cm^{-1} relates to the O–Sn–O bridge functional groups of SnO_2, which confirms the presence of SnO_2 as crystalline phase. This is in agreement with the results of the XRD analysis. With increase doping of antimony (Sb) the peak of 662cm^{-1} almost disappeared that indicates crystalline phase approaches towards amorphous phase. Sb-doped Sno_2 samples have intense and very broad IR no. of peaks ranging from 1300 to 3300cm^{-1}, with four maxima at 1404, 1606, 2359 and 3250cm^{-1}. The peaks at 1404 was assigned to NH deformation of ammonia and NH stretching vibration from decomposition of ammonium hydroxide [29-30]. The intense and broad band's at 1606 and 3250 cm^{-1} can be attributed to the O–H vibration in absorbed water on the sample surface [28,31-33]. This may be due to high surface area of Sno_2 materials results in rapid adsorption of water from the atmosphere because the FTIR samples were kept and ground in air.

3.4 Gas sensing analysis:

The temperature-dependent sensor responses of different samples at different concentration of various gases are shown in fig.4. This sensors response is attributed to chemisorptions of oxygen on oxide surface and the consequent reaction between adsorbed oxygen species and tested gas, which causes the resistance change [34]. The gas responses of these sensors against hydrogen sulphide (H_2S) and ammonia (NH_3) gases were measured at various different operating temperatures to find out their optimum temperatures.

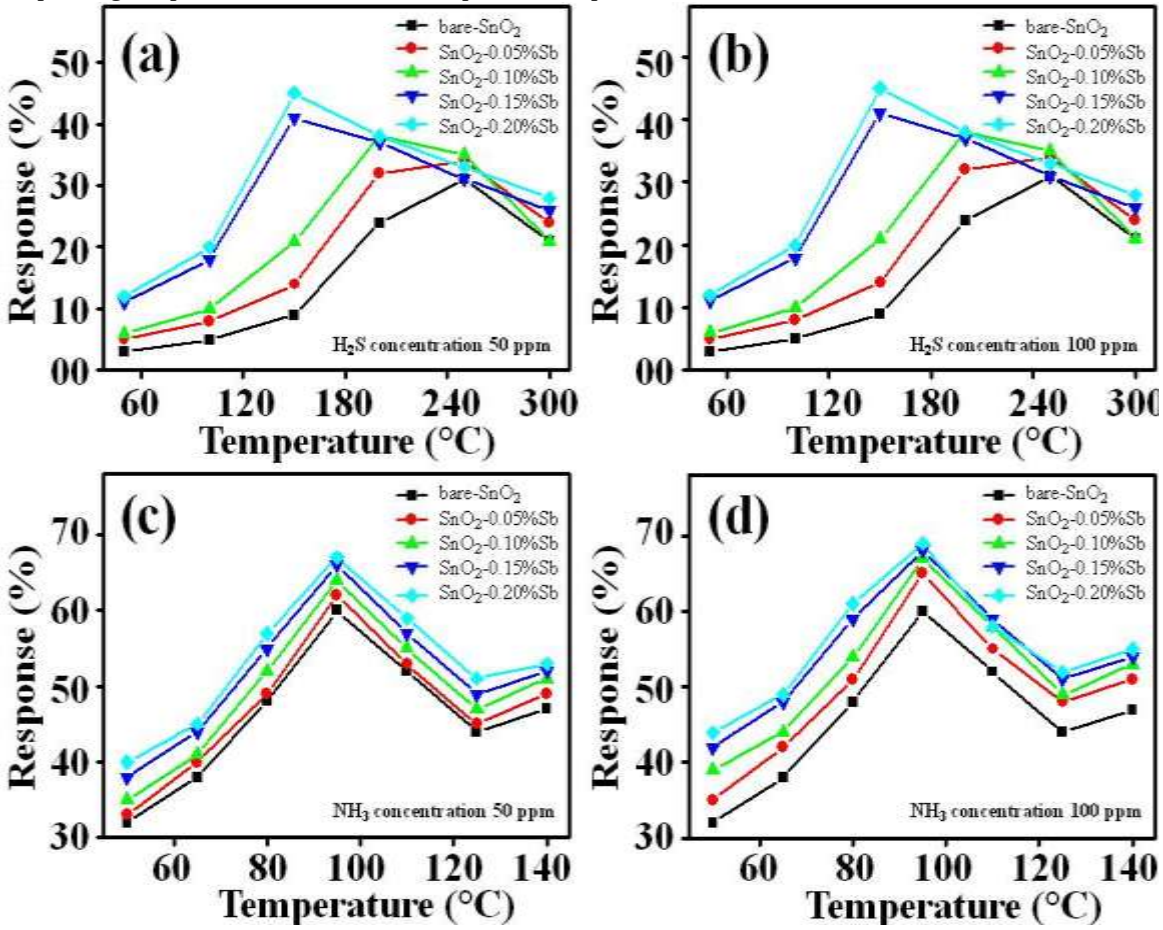

Fig.4 Sensing properties of bare-SnO_2 and Sb-incorporated SnO_2 nanoparticles (x.Sb (1-x). SnO_2 with x=0, 0.05, 0.10, 0.15, 0.20 mol%) towards two different gases: (a-b) H_2S and (c-d) NH_3

The sensors response towards these gases increase at different value of temperature firstly, reach its maximum value at the best possible temperature and then shows decrement with increase in operating temperature. The maximum operating temperature of the prepared sensor of 50 and 100ppm of hydrogen sulphide (H_2S) and ammonia (NH_3) are about 150 and 95^{0}C respectively within the measurement limit.

These temperatures are contributed to the sensor having maximum gas response at corresponding working temperature. For both the concentration 50 as well as 100 ppm of these two gases under consideration, the minimum and maximum gas sensing response was shown by the samples with Sb=0 % (pure tin oxide) and Sb=0.20 % respectively as shown in fig.6.

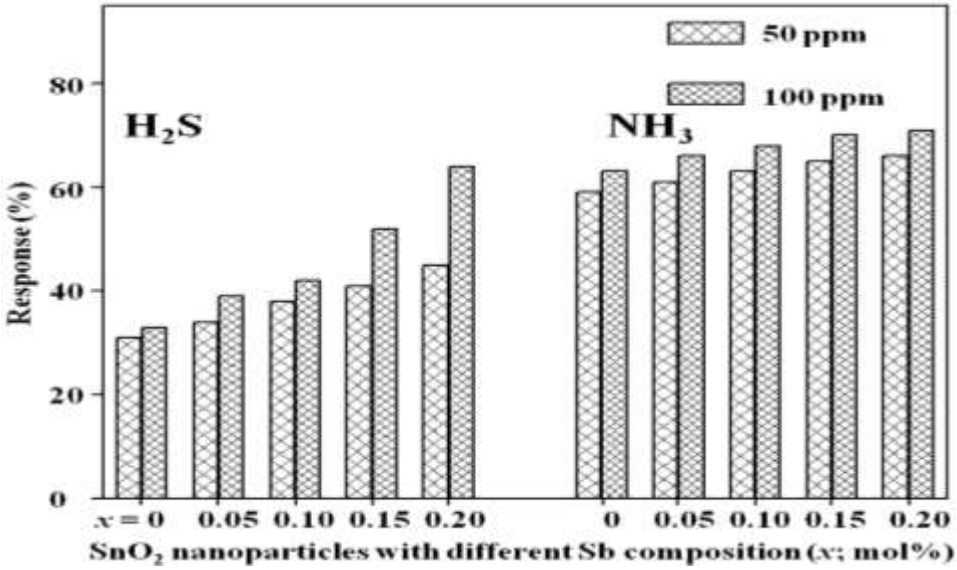

Fig.5 Histograms depicting a comparative study of sensor response for H_2S and NH_3 target gases at different Sb composition (x. Sb (1-x). SnO_2 with x=0, 0.05, 0.10, 0.15, 0.20 mol%)

Table 2 The maximum gas sensor response for H_2S and NH_3 target gases for the bare-SnO_2 and Sb-incorporated SnO_2 nanoparticles.

Samples	**Maximum Response (%) for target gas (at their respective optimal operating temperature)**			
	H_2S		**NH_3**	
x.Sb (1-x).SnO_2	**50 ppm**	**100 ppm**	**50 ppm**	**100 ppm**
x = 0.00	31	33	59	62
x = 0.05	34	39	62	66
x = 0.10	38	42	63	69
x = 0.15	41	52	65	70
x = 0.20	45	64	66	71

It is well known that performance of SnO_2 gas sensor is directly related to its particle size**,** target gas compositional characteristics and nature of dopants (i.e. the presence of additives) [35-38]. In present study the particle size of samples is found to decrease with increase in antimony doping. Therefore, the net increase in sensitivity of the sample under study is attributed to the decrease in particle size as well as increase in antimony content. These results also reveal that Sb-doped SnO_2 nanoparticles show more sensitivity to hydrogen sulphide (H_2S) and ammonia (NH_3) gases in comparison to pure SnO_2 nanoparticles. The results obtained are in good agreements with earlier result published data [39, 40].

Gas sensing data analysis represented in recent scientific literature as well as selectivity of a particular gas sensors can be enhanced by making use of specific additives and developing materials at nanoscale, as it changes electrical properties and create new active sites [41-46].

4. CONCLUSION

Bare and Sb-doped SnO_2 nanoparticles synthesized by hydrothermal technique are found to have tetragonal rutile structure with crystallite sizes in range of 7–21 nm. With incorporation of Sb atoms in the lattice of pure SnO_2 reduction in intensity and broadening of peaks were observed thereby supporting the reduction in the crystallite size. The SEM images of nanoparticles confirms the existence of very small, homogeneously distributed, spherical and extremely crystalline nanoparticles. FTIR study confirmed the formation of Sn–O phase and hydrous nature of Sb-doped SnO_2 nanoparticles.

The gas sensing properties of pure and Sb-doped SnO_2 nanoparticles were investigated for 50 and 100 ppm concentrations of hydrogen sulphide (H_2S) and ammonia (NH_3) at different operating temperatures. In present analysis, the effect of operating temperature on gas-sensing properties of Sb-doped SnO_2 sensors was examined and it has found from fig. 6(c-d) that the operating temperature has a noticeable influence on gas response of sensor to 100 ppm ammonia (NH_3) and hydrogen sulphide (H_2S). Among all samples under study, 0.20% Sb-doped SnO_2 nanoparticles exhibits the best response to these gases.0.20 % Sb-doped SnO_2 nanoparticles showed the maximum response 64 % to hydrogen sulphide (H_2S), and 71% to ammonia (NH_3) at concentration of 100 ppm respectively at different operating temperature within the measurement limit. So it has found that surface functionalization with Sb proven to be an effective way to enhance the performance of SnO_2 nanoparticles gas sensors

REFERENCES: -

[1] M. Epifani, R. Diaz, J. Arbiol, E. Comini, N. Sergent, T. Pagnier, P. Siciliano, G. Taglia and Morante J R. Adv Funct. Mater 16(11):1488–1498, (2006).
[2] S.A. Pianaro, P.R. Bueno, E. Longo and J.A. Varela, J Mater Sci. Lett. 14(10), 692–694, (1995).
[3] S.A. Pianaro, PR Bueno, P. Olivi, E. Longo and JA Varela, J Mater Sci Mater Electron 9(2), 159–165, (1998).
[4] L.H. Jiang, G.Q. Sun, Z.H. Zhou, S.G. Sun, Q. Wang, S.Y. Yan, H.Q. Li, J. Tian, J.S. Guo, B. Zhou and Q. Xin J. Phys Chem B 109(18), 8774–8778, (2005).
[5] Batzill M. Sensors 6(10), 1345–1366, (2006).
[6] M.L. Moreira, S.A. Pianaro, A.V.C. Andrade and A.J. Zara Mater Charact 57(3):193–198 (2006).
[7] A.F. Cabrera, A.M. Mudarra Navarro, C.E. Rodríguez Torres and F.H. Sánchez, Physica B., 398: 215-218 (2007).
[8] Yamazoe, N. *Sens.* Actuat. B. 5 7-19 (1991).
[9] J. Zakrzewski, W. Domanski, P. Chaitas, and Th. Laopoulos, Technology and Applications, Lviv, Ukraine (2003).
[10] M. Anil Kumar, R. Pasricha and V. Ravi, J Ceram Int., 31, 889 (2005).
[11] M.D. Wildberger, J.-D. Grunwaldt, M. Maciejewski, T. Mallat, A. Baiker, Appl. Catal. A, 175, 1 (1998).
[12] S. Gnanam and V. Rajendran, J Sol-Gel Sci Technol., 53, 555, (2010).
[13] A. Cabot, J. Arbiol, R. Ferré, J. R. Morante, Fanglin Chen, J. Appl. Phys., 95, 2178, (2004).
[14] Q. Wan, and T.H. Wang, Chem. Commun., 30, 3841-3843, (2005).
[15] Hyung-Joon Jeon, Min-Kyu Jeon, Misook Kang T, Sung-Gu Lee, Yong-Lae Lee and Young-Ki Hong, Byung-Hyun Choi, Materials Letters 59, 1801–1810, (2005).
[16] F. Bai, Y. He, P. He, Y. Tang and Z. Jia. Materials Letters 60, 3126–3129, (2006).
[17] J. Kong, H. Deng, P. Yang and J. Chu. Materials Chemistry and Physics 114, 854–859, (2009).
[18] A.R. Babar, S.S. Shinde, A.V. Moholkar, C.H. Bhosale, J.H. Kimc, and K.Y. Rajpure. Journal of Alloys and Compounds 509 3108–3115, (2011).
[19] B.D. Cullity, R.S. Stock, Elements of X-ray Diffraction, Prentice Hall, New Jersey, (2001).
[20] R.D. Shannon, Acta Crystallogr. A 32, 751 (1976).
[21] R.K. Mishra and P.P. Sahay, Ceramics International 38, 2295–2304 (2012).
[22] J. Rockenberger, U.zum Felde, M. Tischer, L. Troger, M. Haase and H. Weller, J. Chem. Phys., 112, 4296, (2000).
[23] T. Nutz and M. Haase, J. Phys. Chem. B, 104, 8430 (2000).

[24] T. Krishna kumara, R. Jayaprakash, Nicola Pinna, A.R. Phani, M. Passacantando and S. Santucci. Journal of Physics and Chemistry of Solids 70, 993–999, (2009).
[24] V. Geraldoa, Luis V.A. Scalvi, P.N. Lisboa-Filho and C. Morilla-Santos. Journal of Physics and Chemistry of Solids 67, 1410–1415, (2006).
[26] G. Mulongo, J. Mbabazi and S. Hak-Chol, Res. J.Chem.Sci., 1(4), 18-21 (2011)
[27] J. Zhang and L. Gao, J. Inorg. Chem. Commun. 7, 91-93(2004).
[28] J. Zhang and L. Gao, J. Solid State Chemistry, Vol.177, 4-5, 1425–1430, (2004).
[29] K.C. Song and Y. Kang Mater. Lett. 42, 283-289 (2000).
[30] T. Krishna Kumar, N. P. Kumari, K. P. Perumal and K. Jayaprakash R. J. Mater. Lett. 62, 3437-3440 (2008).
[31] G. L. Zou, R. Liu, W. X. Chen, and Z. D. Xu, Materials Research Bulletin, vol. 42, no. 6, 1153–1158 (2007).
[32] Y. Wang and N. Herron, J. Phys. Chem. 95,525 (1991).
[33] S. Karuppuchamy and J. M. Jeong. J. Oleo Sci. 55, 263 (2006).
[34] H. Gonga, J.Q. Hua, J.H. Wang, C.H. Onga and F.R. Zhub, Sens. Actuators B 115, 247–251 (2006).
[35] W. Göpel and K. D. Schierbaum, Sens. Actuators B 26, 1 (1995).
[36] N. Yamazoe, Sens. Actuators B 5, 7 (1991).
[37] L. Hozer, translation editor D. Holland, Ellis Horwood, New York; PWN-Polish Scientific Publishers, Warsaw, (1994).
[38] C. O. Park and S. A. Akbar, J. Mater. Sci. 38, 4611 (2003).
[39] J. Maa, Y. Liua, H. Z. P. Ai, N. Gonga, Y. Wu and D. Yu Sensors and Actuators B 216, 72–79 (2015).
[40] Yude Wang, Qiuying Mu, Guofeng Wang and Zhenlai Zhou, Sensors and Actuators B 145 847–853, (2010).
[41] S. H. Saeedabad, G. S. Selopal, S. M. Rozati, Y. Tavakoli and G. Sberveglieri, Journal of Electronic Materials, Volume 47, Issue 9, pp 5165–5173 (2018).
[42] S. Nagirnyak and T. Dontsova, Nano Research & Applications ISSN 2471-9838 Vol. 3 No. 2: 8, (2017).
[43] M. Wang, L. Zhu, C. Zhang, G. Gai, X. Ji, B. Li and Y. Yao, Sensors and Actuators B: Chemical Volume 224, Pages 478-484 (2016).
[44] F. Rechberger, R. Städler, E. Tervoort and M. Niederberger, Journal of Sol-Gel Science and Technology Volume 80, Issue 3, pp 660–666 (2016).
[45] M. Narjinary, P. Rana, A. Sen and M. Pal , J. Materials & Design Volume 115, Pages 158-164 (2017).
[46] S. Majumdar , J. Ceramics International Volume 41, Issue 10, Pages 14350-14358 (2015).